Dissection of a composite volcanic earthquake at Santiaguito, Guatemala

J. B. Johnson,[1] R. Sanderson,[1] J. Lyons,[2] R. Escobar-Wolf,[2] G. Waite,[2] and J. M. Lees[3]

Received 4 June 2009; revised 20 July 2009; accepted 28 July 2009; published 28 August 2009.

[1] Volcano earthquake sources associated with eruptions at Santiaguito volcano in Guatemala are complex. Rock fracture, fluid flow, and gas expansion occur at variable time scales and induce superposed ground motions, including both static and dynamic deformation, and atmospheric pressure disturbances. Dissection of this composite event is facilitated through extra-seismic observations, such as infrasound, geodetic, and visual monitoring. Multi-parametric investigation of an eruptive event on Jan. 4th 2009 reveals increased degassing, apparent as both geodetic tilt and harmonic seismo-infrasonic tremor, preceding an explosive event. The explosive event itself entails surface dome uplift, multiple eruptive pulses, and subsequent re-equilibration of the volcanic edifice manifested in derived tilt. We report here on an integrated approach to discerning the physical processes at the actively effusing and exploding Santiaguito volcano and describe the composite earthquake that occurs here. **Citation:** Johnson, J. B., R. Sanderson, J. Lyons, R. Escobar-Wolf, G. Waite, and J. M. Lees (2009), Dissection of a composite volcanic earthquake at Santiaguito, Guatemala, *Geophys. Res. Lett.*, *36*, L16308, doi:10.1029/2009GL039370.

1. Introduction

[2] Descriptive volcano earthquake classifications are often associated with a fundamental source process or processes, which are thought to be dominant. High-frequency (HF) or short-period (SP) events, for instance, are often attributed to brittle failure of rock and are commonly referred to as volcano-tectonic (VT) earthquakes. Long-period (LP) earthquakes are also common at volcanoes and are frequently attributed to fluid flow, which is thought to induce conduit or chamber resonant oscillations [*Chouet*, 1996]. Tremor, in some of its many forms, is considered to be a potential superposition of rapid-fire LPs [*Neuberg et al.*, 2000] while explosion earthquakes come in many flavors and may have clearly identifiable air phases [e.g., *Ripepe and Braun*, 1994]. Finally, very long period (VLP) events and even lower ultra long-period (ULP) events are associated with volumetric sources and, as their name implies, are associated with long-duration (tens to hundreds of s and more) source movement [e.g., *Neuberg et al.*, 1994; *Kawakatsu et al.*, 2000].

[3] Many volcanic earthquakes are not easily ascribed to just one of these categories, however. Hybrids have been recognized as amalgams of HF and LP [*Lahr et al.*, 1994], whereas explosion events often include integrated VLP, LP, HF energy, and tremor [e.g., *Ohminato and Ereditato*, 1997; *Nishimura et al.*, 2000; *Aster et al.*, 2008]. Here we present observations and analysis from Santiaguito volcano (Guatemala) where complex earthquakes associated with eruptions persist for several minutes before dropping to background levels. Although previous studies in 2003 and 2007 focused on combined seismic, acoustic, and thermal radiation during eruptive events [*Johnson et al.*, 2004; *Sahetapy-Engel et al.*, 2008], the 2009 data yielded broader band seismic and infrasonic data and concurrent audio-visual footage from stations close to the vent. Throughout the 2009 study, HF and SP energy, LPs, VLPs, ULPs, and several types of tremor appear overprinted during eruptive events. We report on one of these complex 'composite' events and comment on the temporal linkage of its various physical source processes.

2. Background

[4] Santiaguito's dome complex has been active since 1922, building four named domes with cumulative volume of $\sim$1.5 km^3 [*Durst*, 2008]. Since 1967 Caliente Dome, farthest to the SW, has been the primary locus of explosive eruptions and, often concurrent, lava effusion [*Rose*, 1987]. During visits by our research team and colleagues from 2003 to 2009 activity was roughly comparable, with active andesite-dacite [*Avard et al.*, 2006] block lava flow spalling off the dome to the east, south, and/or southwest as intermittent rockfall and small volume pyroclastic flows. Pyroclastic and ash-laden explosive eruptions were frequent (>10 per day) and reached more than 1 km above the vent. In January 2009, eruption recurrence intervals averaged 1.5 hours, but these explosions were energetic (compared to 2007, for instance) in that they endured for up to 10 minutes and regularly sent ash columns that extended above Santa Maria summit, 1200 m above the vent.

[5] The 2009 deployment included 4 broadband seismometers and 6 acoustic pressure transducers distributed around the active vent (Figure 1). The stations operated continuously from January 1–4 recording at 100 Hz with 24-bit resolution and GPS timing. Broadband seismometers included 30-s CMG 40-Ts (at CAR and DOM) to 60 s CMG 3-ESP (at CAL and CAM). Acoustic sensors were ±250 Pa dynamic range All Sensors™ differential pressure transducers with flat passband above $\sim$50 s. Station CAR had

[1]Earth and Environmental Science, New Mexico Institute of Mining and Technology, Socorro, New Mexico, USA.
[2]Geological and Mining Engineering and Sciences, Michigan Technological University, Houghton, Michigan, USA.
[3]Department of Geological Sciences, University of North Carolina, Chapel Hill, North Carolina, USA.

0094-8276/09/2009GL039370

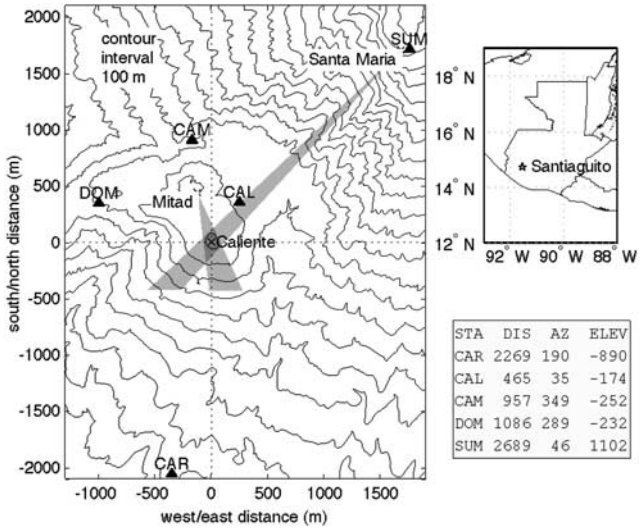

Figure 1. (left) Map showing seismo-infrasound stations from January 2009. Shaded regions indicate approximate fields of view for cameras deployed at Mitad and Santa Maria. (bottom right) Slant distances (m), azimuths, and relative elevations (m) from stations to Caliente Vent. (top right) Santiaguito locator map.

1 microphone, while DOM, CAM, and CAL housed 2-element arrays, and SUM and CAS (off the Figure 1 map to the South) consisted of 3-element arrays with ~15 m spacing between sensor nodes.

[6] Video cameras targeted the active vent during the deployment to aid with seismo-infrasound interpretation. We deployed high-resolution (1920 × 1080 pixel) Casio™ FH-1 cameras at vantage points near the summit of Santa Maria trained on the vent region. The cameras recorded during the mornings of 1–4 Jan. when visibility was clear. An additional 1920 × 1080 pixel Sony™ HDR-SR7 video camera with microphone operated at Mitad Dome (400 m NNW from the vent) in night-vision mode and recorded nighttime activity on 3–4 Jan. Camera clocks were time-synced with handheld GPS units such that video timing is accurate to within ±1 s.

[7] On 3 January at 21:49 local time (03:49 GMT on 4 January) we recorded an explosive eruption with nighttime video and audio, 12 seismic channels, and 13 infrasound channels. We focus on this event because of the high-quality video and low wind noise contamination on audio and infrasound channels across our network. The event ranked relatively large in terms of size; its peak seismic amplitude was 10 of 58 for all eruption events recorded during a 90 hour interval. Bracketing eruptive events of comparable size occurred 1.6 hours previously, and 2.9 hours afterwards.

3. Analysis

[8] The eruption produced broadband seismic and acoustic emissions that appear to reflect diverse physical sources occurring at different times and time scales. In order to characterize these mechanisms, we examined multiple band-limited elastic wave records (Figure 2). We filtered the seismic and infrasound data into 5 non-overlapping bands to provide focus on waveform features that may otherwise be hidden. Bandpass corners roughly mimic established volcano seismic frequency bands and for convenience we informally refer to the corresponding filtered waveforms as ULP (600 to 30 s), VLP (30 to 5 s), LP (5 s to 1 s), SP (1 Hz to 10 Hz), and HF (10 Hz to 50 Hz). We use the same nomenclature for infrasound frequency divisions. Data were filtered with a two-pole minimum phase causal Butterworth filter. Except for traces displayed in Figures 2i and 2j, seismometer response was removed down to 600 s.

[9] Horizontal components on near field sensors are susceptible to tilt (θ) as gravity accelerates the seismometer mass in the downdip direction, which can be indistinguishable from updip horizontal ground motion [e.g., *Wielandt and Forbriger*, 1999; *Aoyama and Oshima*, 2008]. We believe the horizontal Santiaguito ULP signal is most likely a tilt artifact because horizontal motion is so dominant at the 3 closest seismic stations; at CAL, for instance, the principle component ULP eigenvector dips at only 1°. To examine this effect, consider that a Mogi source would have a horizontal displacement canceled by tilt-associated acceleration at a period of $T = \sqrt{\frac{4\pi^2}{3g}\frac{\left(r^2+z_0^2\right)}{z_0}}$ (see auxiliary material).[1] For CAL's horizontal distance of r = ~400 m and for an arbitrary source depth range of 200 m < z_0 < 800 m the absolute influences of Mogi-induced translation and rotation will be equal at 33 s < T < 37 s, with tilt becoming quadratically more influential at longer periods. We converted ULP radial signal at CAL to an inferred 'pseudo-tilt' in part because of the dominance of energy several octaves below this period. Tilt displayed in Figure 2o comes from the ULP pass-band signal following instrument response deconvolution, conversion to acceleration, and inverse scaling of gravity $1/g$ (see auxiliary material).

[10] We use observations from video and audio streams from the Mitad camera to constrain the geophysical data associated with the featured event. Night-mode digital video is converted to a qualitative eruption flux time series by averaging pixel intensity in each image frame. Incandescent emissions of bombs and ash show up with high brightness values serving as a proxy for eruptive vigor. Video of the event is provided at two different durations (10 and 1 minute) and play speeds (×50 and ×1) along with seismic-infrasound traces and audio tracks (see auxiliary material).

[11] The notable feature of the incandescence time series is a sharp increase in average pixel brightness occurring at 3:47:11.5 GMT ± 1 s, a time we hereon refer to as the eruption onset at 0 s. This uptick is associated with onset of a pyroclastic-laden eruption and this time divides "pre-eruptive" and "post-eruptive" phases. The video-derived time series is accurate to ±1 s and is presented in Figure 2 on a common time axis with the seismo-infrasound data. No time shift for elastic wave transmission is applied, however we refer to all phase arrivals relative to 0 s as source-time adjusted. This adjustment assumes that sound propagation

[1] Auxiliary materials are available in the HTML. doi:10.1029/2009GL039370.

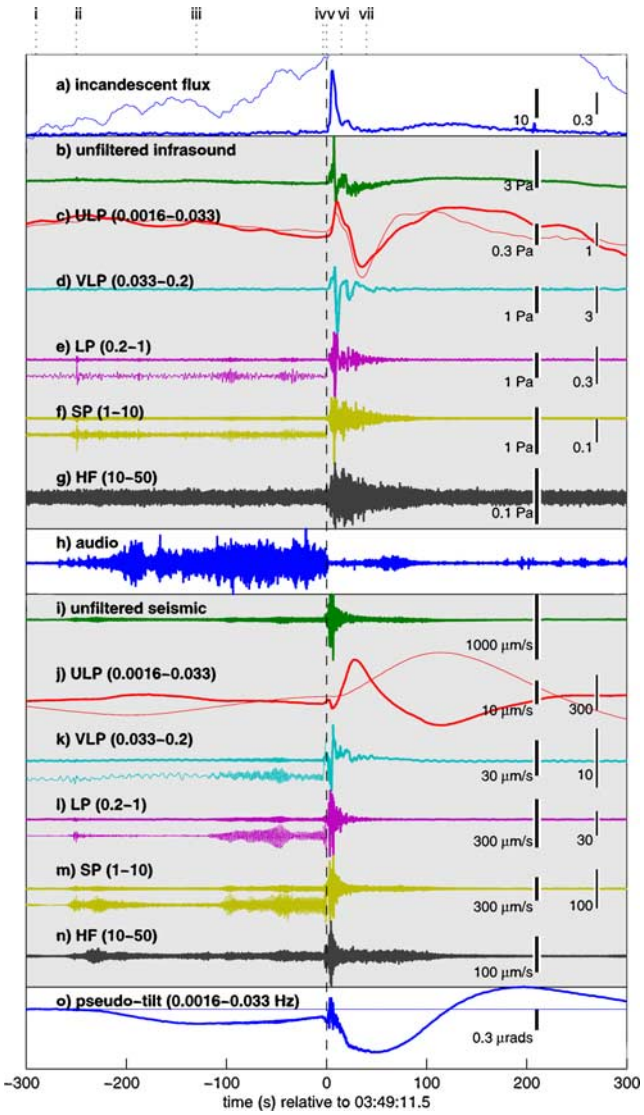

Figure 2. Time series records of video-audio and seismo-infrasound-tilt. Detail of this figure is provided in auxiliary materials. Trace data shown as bold lines include: (a) incandescent time series extracted from Mitad camera video, (b–g) unfiltered and band-filtered infrasonic pressure at CAM, h) audio trace recorded by Mitad camera, (i–n) unfiltered and band-filtered horizontal radial seismic velocity at CAL, (o) inferred tilt extracted from band-limited (600 to 30 s) radial seismic. Thin lines for select data fields indicate: amplified incandescent time series (Figure 2a), ULP and VLP infrasound recorded at station CAL (Figures 2c–2d), amplified pre-eruptive tremor (Figures 2e and 2f), instrument-deconvolved ULP velocity trace (Figure 2j), amplified pre-eruptive seismic tremor (Figures 2k and 2l), and zero tilt ordinate (Figure 2o). Note different scale bars for thin line trace data. Indicated times of interest, which are highlighted in text, include: (i) initial increase in incandescence, (ii) seismo-infrasound transients, (iii) harmonic tremor onset, (iv) 'pre-explosion' seismicity, (v) explosion visible at vent, (vi) secondary explosive pulse, and (vii) return of audible jetting sounds.

from the Caliente source region is 330 m/s and seismic propagation is ~1500 m/s.

4. Pre-eruptive Seismo-acoustic Characteristics

4.1. Video and Audio

[12] At the beginning of recorded video, which we started to film more than six minutes prior to eruption, incandescent glow is barely perceptible from the Caliente vent, however starting at ~−290 s (i) it gradually increases (see amplified trace in Figure 2a). At the same time jet noise, which was barely noticeable from Mitad at the start of the video, becomes pronounced. For nearly 4 minutes, incandescence and audible sound intensity increase before audio levels peak at −22 s and decay to background by +1 s.

4.2. Infrasound

[13] Compared to the intense broadband infrasound after eruption, the pre-eruptive infrasound is low intensity and evident in limited bands. Pressure levels are most energetic in the LP-band (0.01 to 0.04 Pa RMS at CAM and CAL) for the 300 s leading up to eruption. HF recordings are completely obscured in the ~3–4 mPa RMS instrument noise floor. Potential pre-eruptive VLP and ULP infrasound signals are also below the noise floor. Despite its low amplitude, pre-eruptive sound in the LP and SP bands is well correlated across network stations DOM, CAM, and CAR. Infrasound radiation commences with a short (few s) infrasound transient (0.5 to 1 Pa peak-to-peak) identifiable at −253 s (ii). Following this at −128 s (iii) a monotonic infrasonic tremor (0.43 Hz) is seen in the LP and SP bands. It modulates several times before leading uninterrupted to the eruption itself.

4.3. Seismic

[14] Both the infrasonic transient at −253 s (ii) and the infrasonic harmonic tremor beginning at −128 s (iii) are manifested in the pre-eruptive seismic records in the VLP to SP bands. The onset of a discrete seismic event appears at −258 s (ii) and the pre-eruptive seismic harmonic tremor is emergent beginning around −125 s (iii). Tremor persists for at least two minutes with striking consistency in its fundamental frequency that is shared by the infrasound (0.43 Hz). Notably, the seismic harmonic tremor has ~10 additional well-defined integer overtones at 0.86, 1.29, 1.72, and 2.15, etc. Spectral amplitudes for the 2nd and 4th harmonics are diminished as predicted by flow-induced tremor models [*Julian*, 1994]. Given the conjoint nature of the acoustic and seismic signals, it is likely that the tremor is related to shallow fluid flow.

[15] The HF seismic signal that emerges after the −258 s transient is cigar-shaped with its highest amplitude pulse (~50 um/s) occurring at −240 s, diminishes in amplitude between −200 to −160 s, and increases again a few s prior to eruption. HF signals increase during the eruption and retain a cigar-shaped form before tapering at +120 s. Spectral content, amplitude, and envelope of the HF signal starting at about ~240 s and again at ~0 to 120 s suggest sustained rock falls from the block lava flow, which are common at Santiaguito at any time, but is frequently instigated during eruptive events. Although the audio record is dominated by jetting sound prior to 0 s, and thus obscures

potential noise of rock fall, ballistic impact and rock fall are clearly audible following the eruption onset.

4.4. Pseudo-tilt

[16] 'ULP-band seismicity' is converted to tilt and is noticeable beginning at about −250 s (ii). Its onset is gradual, but is roughly coincident with the initial discrete seismo-infrasound transient and concurrent increase in incandescent material flux and audio jetting. Assuming a Mogi-type source beneath the Caliente Vent and a half-space geometry, the tilt is down toward the source indicating deflation. Equivalent cavity volume loss can be quantified as $\Delta V = -\theta \frac{4\pi}{9} \frac{\left(r^2+z_0^2\right)^{5/2}}{r z_0}$ where the minimum Mogi source cavity volume is found at $z_0 = r/2$ (see auxiliary material). For r = 400 m, z_0 = 200 m, and pre-eruptive tilt of 0.3 micro-radians the required volume loss is ∼100 m^3. A study of depth-dependent Mogi volume size is left to future study.

5. Post-eruptive Seismo-acoustic Characteristics

5.1. Video and Audio

[17] The emission of incandescent material at 0 s (v) coincides with a striking cessation of audio signal by 0.5 s (Figure 2h). Assuming that the termination of this audio is a source phenomenon, and not an artifact of enhanced acoustic attenuation in an ash-rich plume, we attribute the jetting diminution to opening of surface fractures during the onset of the co-eruptive phase. Audio energy remains mostly absent until ∼40 s (vii) when it reappears in association with renewed gas jetting and then terminates at ∼90 s.

5.2. Infrasound

[18] Intense infrasound at the onset of eruption radiates with peak-to-peak unfiltered amplitude of 10 Pa at CAL and 5 Pa at CAM. Infrasound is similarly intense in ULP, VLP, and LP bands and is diminished in the SP and HF bands. In all bands, infrasound endures for more than 60 s corresponding to explosive emissions as seen in the video. Particularly striking is the ULP-band infrasound recorded across the network of microphones. This signal has substantial amplitude (∼1 Pa) as low as ∼100 s.

[19] The most significant VLP infrasound pulse begins at 0 s (v) and is followed by a smaller infrasonic concussion evident from +10 to +20 s (vi). This second pulse is subtly evident in the video record, which shows a second explosive pyroclatic emission. It is broader in time and reduced in amplitude relative to the first explosive emission, due in part to obfuscation by previously-erupted plume. LP and SP-band infrasound is well correlated across the network in short (∼3 s) windowed segments. Correlated LP/SP phases are locatable across a ∼10,000 m^2 area centered at the Caliente summit [*Jones et al.*, 2008], and they show spatial progression over 60 s corresponding to presumed loci of the most vigorous erupting vents.

[20] Co-eruptive HF acoustic signal is diminished in intensity relative to lower frequency bands, however it remains above background to +∼100 s, longer than SP, LP, and VLP infrasound. Higher frequency infrasound, and HF acoustic signal in particular, is less well correlated across the network and we are not able to map HF acoustic energy as a succession of discrete point source radiators. It is possible that the HF energy reflects gas jetting [e.g., *Woulff and McGetchin*, 1976; *Matoza et al.*, 2009], which would not correlate well over a distributed infrasound network. The HF source is fundamentally different than the higher amplitude VLP, LP, and SP infrasound, which are likely caused by volumetric gas expansion.

5.3. Seismic

[21] Although the raw seismic signal emerges from the pre-eruption harmonic tremor, a more rapid increase in seismic energy becomes evident (most notably in the VLP and HF) bands at ∼−3 s (iv), just prior to the 'eruption onset'. This seismicity appears to precede both the source time of the primary infrasound pulse and the incandescent time series inflection by a couple of seconds. SP and HF seismicity increases again at +3 s concurrent with the onset of ballistic impacts, which are evident in the camera video and audio. Another pulse of energy after ∼10 s (vi) is seen in the SP and LP and we hypothesize that it is related to the second explosive emission event identified in video and with infrasound.

[22] VLP-band seismicity begins just a few seconds prior to incandescent emissions and its timing is in agreement with the model of *Johnson et al.* [2008] where rapid (2−3 s) dome uplift was correlated with LP/VLP band seismic radiation. Video of 2009 eruptions also show similar rapid uplift of the dome at the onset of eruptions during which fractures co-incidentally open and the explosive eruption commences. Considering the viewing geometry from the Mitad camera, which is slightly below the level of the Caliente Vent, we expect incandescent emissions to cross the camera's field of view a few s after the onset of the uplift-associated earthquake.

5.4. Pseudo-tilt

[23] ULP-derived tilt shows a clear downward inflection starting at about ∼5−10 s. This signal is radial and horizontal and well recorded on the 3 closest stations. Rapid amplitude decay suggests an elastostatic wave with cumulative 0.6 micro-radian tilt (downward toward source) by +50 s. Inferred Mogi-source volume decrease is highly sensitive to source depth, but could be as small as 200 m^3 for a point source at $z_0 = r/2$ = ∼200 m (see auxiliary material). Notably the tilt starts to recover at about the same time that LP and SP infrasound terminates, at ∼40−60 s suggesting that the observed edifice deflation is directly tied to explosive emissions. It should be recalled that the pseudo-tilt, and corresponding volume change estimate, is sensitive to the seismometer deconvolution. If, for example, we consider ULP signal down to 0.005 Hz then cumulative tilt is only 0.4 micro-radian and responsible volume change could be as small as 133 m^3.

6. Composite Earthquake Summary

[24] Band-limited observations of seismic radiation, infrasound radiation, and video (summarized in auxiliary material in Table S1) provide a fuller picture of the 'peri-eruptive' earthquake behavior at Santiaguito. The analyzed event is more than 8 minutes in duration and comprises ∼4 minutes of a pre-eruptive seismo-acoustic activity, which coincides with increasing fumarolic jetting and gradual opening of near-surface fractures. Pre-eruptive tremor is notably

punctuated by discrete seismo-acoustic pulses and, starting two minutes before the eruption, near-surface harmonic tremor that is evident in both the seismic and infrasonic wavefields.

[25] Vigorous gas jetting terminates coincidently with the onset of LP and VLP seismic radiation resulting from rapid dome inflation, fracturing, and decompression. Gases are tapped from magma exposed in fissures, which extend over the vent region. Individual eruptive pulses, including at least two significant sub-events, are seen in both seismic and infrasound SP and LP channels. Inferred vent-directed downward tilt is noted with the onset of pre-eruption degassing activity, but accelerates within about 10 s of the onset of the eruptive period. This deflation is induced by depressurization and/or evacuation of material in the conduit. The audio channel provides evidence for jetting that returns to the vent region several tens of seconds after the eruption onset, but decays to background within about 100 s after the eruption. This jetting is speculatively associated with progressive constriction and annealing of fractures as gas flow diminishes prior to the next inter-eruptive quiescent cycle.

7. Conclusion

[26] The highlighted event originates from a complex superposition of sources that do not neatly belong to any traditional volcano earthquake category. We treat this event as a single discrete earthquake because it comprises interdependent and continuing physical sources including vigorous near-surface fluid flow, surface degassing, eruptive explosions, induced rock fall, rapid dome uplift, and edifice deflation. Analysis of other Santiaguito seismic eruption signals reveals that most events contain a subset of the features highlighted above. Our preliminary interpretation of this complex earthquake is facilitated by the deployment of broadband and high-dynamic range seismometers and microphones deployed close (<1 km) to the sources. Sensitivity in the LP, VLP, and ULP bands reveals a variety of slower source processes that would go unnoted with more restricted-band sensors. Future exploration at Santiaguito could benefit from even longer-period and rotational seismometers and dedicated geodetic sensors in addition to other audio-visual observations.

[27] **Acknowledgments.** We are grateful for support from INSIVUMEH (through G. Chigna), the Policía Nacional Civil de Guatemala and the Instituto Guatemalteco de Turismo (through C. Barrio), K. Brill, J. Anderson, C. Forbes, E. Lopez, A. Miller, and J. Silverman. This work was possible through financial support from NSF EAR 0738802, NSF EAR 0838562, and NSF PIRE 0530109.

References

Aoyama, H., and H. Oshima (2008), Tilt change recorded by broadband seismometer prior to small phreatic explosion of Meakan-dake volcano, Hokkaido, Japan, *Geophys. Res. Lett.*, *35*, L06307, doi:10.1029/2007GL032988.

Aster, R., et al. (2008), Moment tensor inversion of very long period seismic signals from Strombolian eruptions of Erebus Volcano, *J. Volcanol. Geotherm. Res.*, *177*, 635–647, doi:10.1016/j.jvolgeores.2008.08.013.

Avard, G., A. Whittington, W. Rose, O. Matias, and J. Cornejo (2006), Domes and flows: Do temporal trends in dacitic magma chemistry and rheological behavior at Santiaguito, Guatemala, reflect magma chamber or conduit processes?, *Eos Trans. AGU*, *87*(52), Fall Meet. Suppl., Abstract V51E–1718.

Chouet, B. A. (1996), Long-period volcano seismicity: Its source and use in eruption forecasting, *Nature*, *380*, 309–316, doi:10.1038/380309a0.

Durst, K. (2008), Erupted magma volume estimates at Santiaguito and Pacaya Volcanoes, Guatemala, M.S. thesis, Mich. Tech. Univ., Houghton.

Johnson, J. B., A. J. L. Harris, S. T. M. Sahetapy-Engel, R. Wolf, and W. I. Rose (2004), Explosion dynamics of vertically directed pyroclastic eruptions at Santiaguito Volcano, *Geophys. Res. Lett.*, *31*, L06610, doi:10.1029/2003GL019079.

Johnson, J. B., et al. (2008), Long-period earthquakes and co-eruptive dome inflation see with particle image velocimetry, *Nature*, *456*, 377–381, doi:10.1038/nature07429.

Jones, K. R., J. B. Johnson, R. C. Aster, P. Kyle, and W. McIntosh (2008), Using infrasound to locate eruptive sources at Erebus and Santiaguito volcanoes, *Eos Trans. AGU*, *89*(53), Fall Meet. Suppl., Abstract V51C–2054.

Julian, B. R. (1994), Volcanic tremor: Nonlinear excitation by fluid flow, *J. Geophys. Res.*, *99*, 11,859–11,877, doi:10.1029/93JB03129.

Kawakatsu, H., et al. (2000), Aso94: Aso seismic observations with broadband instruments, *J. Volcanol. Geotherm. Res.*, *101*, 129–154, doi:10.1016/S0377-0273(00)00166-9.

Lahr, J. C., et al. (1994), Earthquake classification, location, and error analysis in a volcanic environment: Implications for the magmatic system of the 1989–1990 eruptions at Redoubt Volcano, Alaska, *J. Volcanol. Geotherm. Res.*, *62*, 137–151, doi:10.1016/0377-0273(94)90031-0.

Matoza, R., et al. (2009), Infrasonic jet noise from volcanic eruptions, *Geophys. Res. Lett.*, *36*, L08303, doi:10.1029/2008GL036486.

Neuberg, J., R. Luckett, M. Ripepe, and T. Braun (1994), Highlights from a seismic broadband array on Stromboli Volcano, *Geophys. Res. Lett.*, *21*, 749–752, doi:10.1029/94GL00377.

Neuberg, J., et al. (2000), Models of tremor and low-frequency earthquake swarms on Montserrat, *J. Volcanol. Geotherm. Res.*, *101*, 83–104, doi:10.1016/S0377-0273(00)00169-4.

Nishimura, T., H. Nakamichi, S. Tanaka, M. Sato, T. Kobayashi, S. Ueki, H. Hamaguchi, M. Ohtake, and H. Sato (2000), Source process of very long period seismic events associated with the 1998 activity of Iwate Volcano, northeastern Japan, *J. Geophys. Res.*, *105*, 19,135–19,147, doi:10.1029/2000JB900155.

Ohminato, T., and D. Ereditato (1997), Broadband seismic observations at Satsuma-Iwojima Volcano, Japan, *Geophys. Res. Lett.*, *24*, 2845–2848, doi:10.1029/97GL02903.

Ripepe, M., and T. Braun (1994), Air-wave phases in strombolian explosion-quake seismograms: A possible indicator for the magma level, *Acta Vulcanol.*, *5*, 201–206.

Rose, W. I. (1987), Volcanic activity at Santiaguito Volcano, 1976–1984, *Spec. Pap. Geol. Soc. Am.*, *212*, 17–27.

Sahetapy-Engel, S., et al. (2008), Thermal, seismic and infrasound observations of persistent explosive activity and conduit dynamics at Santiaguito lava dome, Guatemala, *J. Volcanol. Geotherm. Res.*, *173*, 1–14, doi:10.1016/j.jvolgeores.2007.11.026.

Wielandt, E., and T. Forbriger (1999), Near-field seismic displacement and tilt associated with the explosive activity of Stromboli, *Ann. Geofis.*, *42*, 407–416.

Woulff, G., and T. R. McGetchin (1976), Acoustic noise from volcanoes: Theory and experiment, *Geophys. J. R. Astron. Soc.*, *45*, 601–616.

R. Escobar-Wolf, J. Lyons, and G. Waite, Geological and Mining Engineering and Sciences, Michigan Technological University, 1400 Townsend Drive, Houghton, MI 49931, USA.

J. B. Johnson and R. Sanderson, Earth and Environmental Science, New Mexico Institute of Mining and Technology, 801 Leroy Place, Socorro, NM 87801, USA. (jeff.johnson@ees.nmt.edu)

J. M. Lees, Department of Geological Sciences, University of North Carolina, Campus Box 3315, Chapel Hill, NC 27599-3315, USA.